Iraqi Journal of Physics, 2024
https://doi.org/10.30723/ijp.v22i2.1167

Vol. 22, No. 2, PP.57-68
P-ISSN: 2070-4003
E-ISSN: 2664-5548

Study of the Optical and Structural Properties of Metal-Doped Titanium Dioxide Electrode Prepared by the Sol-Gel Method for Dye-Sensitized Solar Cells

Hadeel D. Hamadalla[1a*] and Falah H. Ali[1b]
[1]*Department of Physics, College of Science, University of Baghdad, Baghdad, Iraq*
[b]E-mail: falah.Ali@sc.uobaghdad.edu.iq
[a*]Corresponding author: hadeeldakheel6@gmail.com

Abstract

This study presents a strategy to increase the efficiency of dye-sensitized solar cells (DSSCs) by doping titanium dioxide (TiO_2) with different magnesium (Mn) concentrations (1, 3, 5, 7, and 9%) generated by the sol-gel process and effectively employed as a photo-anode (the working electrode) for DSSCs. The Doctor Blade method coated the indium-doped tin oxide (ITO) glass with a thin film layer. X-ray diffraction (XRD) was used to evaluate the characteristics of undoped and manganese-doped TiO_2, and the results demonstrate that all of the thin films are anatase. The samples were examined using XRD to assess grain size before and after Mn doping. The spectrum of UV-Vis absorption changes; accordingly, as doping increases, the energy gap decreases. The smallest energy gap's value (2.4 eV) is 7% manganese doping. AFM pictures show the average roughness and root mean square of the weight percentage of films doped with 5%. Field effect scanning electron microscope (FE-SEM) studies show that the particle size of thin films gets smaller as more Mn is added, which happens at least as much as 7% Mn doping. The optimal thickness for TiO_2 paste over conductive glass is 15 µm, and the cell's power conversion efficiency increased to 0.604074% with an Imax of 4.965 mA, a V_{max} of 0.488 V, and a fill factor (FF) of 68.45954%.

Article Info.

Keywords:
DSSC, Mn- doping, Rhodamine B, TiO_2, Fill Factor.

Article history:
Received: Jul. 03, 2023
Revised: Nov.10, 2023
Accepted: Nov.14, 2023
Published: Jun. 01, 2024

1. Introduction

Dye-sensitized solar cells (DSSCs) gained progress in 1991 because of their low cost, simple fabrication method, good stability, and high conversion efficiency. Recently, doping titanium dioxide (TiO_2) with nano mental and metal elements was seen as a promising method to customize the TiO_2 photo anode's electronic properties in DSSCs. This method was successful in enhancing DSSCs' photovoltaic (PV) performance [1]. Extensive research is being done on DSSCs. Also, DSSCs are especially appealing for creating integrated PV cells since the device's color may be changed easily by choosing various cells and dyes on flexible substrates shown already [2]. The DSSCs consist of a photoanode (semiconductor with adsorbed dye molecules), counter electrode (thin layer of redox catalyst), and electrolyte in the inter-electrode space (made of organic solvent with redox mediator) [3]. Electrolytes are crucial in determining how well a cell performs. Generally, using an electrolyte along with the right additions increased the conversion efficiency regarding DSSC. To improve open-circuit photovoltage (V_{oc}) and therefore conversion efficiency (η) of DSSC, additives are added to the electrolytes [4]. The electrolyte solution has an important role in obtaining high efficiency of adding suitable chemicals, and its usefulness to enhance open circuit. As a result, increased efficiency (η) in DSSC [5]. Found highest value efficiency of ruthenium with a base TiO_2

film reached 11%–12%, but became undesirable because of its high cost [6]. The research interest in nanostructured TiO_2 thin films is rapidly rising due to its numerous and potential applications, such as photo catalysis, photonics, optoelectronics, electrochemistry, and photo electrochemistry [7]. Titanium dioxide exists as anatase, rutile, and brookite. Although rutile is the most widespread and stable form of titanium dioxide, anatase is preferred for its high photocatalytic activity [8]. Doping can be made homogenous from the initial solution or restricted to the nanoparticle surface. The metal ions can narrow the TiO_2 band gap by introducing discrete energy levels within the forbidden gap or contribute to the separation of photo-generated charges (e^-/h^+) by capturing the electrons. Even though adding transition metal ions (Mn) to TiO_2 can increase its photocatalytic efficiency, other variables related to the synthesis process and the final catalyst's physical properties affect this material's activity. One of the proposed methods for producing TiO_2 in literatures [9, 10] The Photocatalysis process is based on the irradiation by photons of energy equal to or greater than their bandgap energy of semiconductor particles that transmits the electron from the valence band (VB) to the conduction band (CB), thus creating an electron-hole pair [11]. When photons with energy (hν) equal to or greater than the semiconductor with bandgap (E_g) are incident, electrons and holes are created in the conduction band and valence band [12]. The simplest description of the solar cells uses photovoltaic technology to turn sunlight directly into electricity. It is based on two theoretical parameters: the loss of charge carriers through so-called recombination mechanisms and the generation of current by absorbing incident illumination [13]. Metal oxides are compounds that contain at least one metal and one oxygen ion in their chemical formula such as ZnO, Fe_3O_4, TiO_2, Al_2O_3, $BaTiO_3$, and $BaZrO_3$. They play an important role in the fields of chemistry, physics, and materials science [14] is a particularly appealing method for introducing foreign metal ions into TiO_2 films and powders, Titanium dioxide is widely utilized in a variety of applications, including (DSSCs) dye-sensitized solar cells, water and air purification self-cleaning [15].

The purpose of this work is to increase the charge carriers in dye sensitized solar cells by increasing active charge carriers to the electrode and so increasing their efficiency.

2. Experimental Work

2.1. Materials

TiO_2 powder anatase at 38 nm was prepared. Acetic acid 1-Propanol CH_3CH_2OH (assay 99.80%) with deionized water, manganese $MnCL_2$. $4H_2O$, (undoped 97%), Ti $[OCH\ (CH_3)_2]^4$, titanium tetraisopropoxide (TTIP) Potassium iodide (KI), iodine (I2), acetic acid solution, ethanol, and acetic acid were used in this study.

Also used are: conductive glass coated with ITO (resistance 11 Ω/sq), organic solvent-based electrolyte, dye Rhodamine B, distilled water, sealing agent acetone (transmission (80%)), sheet resistance (11 Ohm/sq), Chinese TES1333 digital radiation detector used as a solar power meter. The DSSC - China's open-circuit photovoltage and short-circuit photocurrent were measured using a digital multimeter.

2.2. Experimental Procedure

The working electrode was prepared by applying the TiO_2 paste to an ITO conductive glass using the doctor-blade approach. The thickness of the titania layer was measured using Scotch tape that was applied to the left and right sides of the substrate's conductive glass face and had a thickness of 15 μm. After that, the Scotch tape was removed, and the films were placed in a covered Perti dish to dry for 30 minutes. The films were then annealed at 550^{o}C for 30 mins in an ambient environment. Lastly, the

working electrode was cooled to room temperature. It was then immersed in a 0.25 mg Rhodamine B dye solution for 24 hours. A similar procedure was used to prepare the working electrode. Two holes of 1 mm diameter were drilled in a second ITO conductive glass on which carbon paste was applied on its conductive side to prepare the counter electrode. Carbon paste was applied using the Doctor-blade approach, and the electrodes were annealed at 550°C for 30 mins in an ambient atmosphere. As a result, carbon is evenly distributed and exhibits strong catalytic activity. The counter electrode was placed on top of the working electrode, with the carbon film facing the TiO_2 paste side of the working electrode. A sealant gasket with a spacer of 30 μm thickness was used to sandwich the working electrode and counter electrode together. Lastly, a pipette was used for injecting some drops of electrolyte through the counter electrode's holes in the contact area between the two glasses, and a plaster to prevent evaporation sealed the holes. The electrolyte was evenly dispersed over the stained TiO_2 film through capillary action. Using tissue or cotton, extra electrolyte from the exposed part of the glass was removed using tissue or cotton. The working electrode was prepared from TiO_2 and from Mn-doped TiO_2. In both cases, the entire cell was exposed to sunlight to generate energy, and efficiency was calculated.

2.3. Assembly and Measurements of the Solar Cells

The electrodes were gathered face to face to keep the TiO_2 coated surface and the carbon coated face in touch with the electrolytes in between. The electrolyte was spread evenly throughout TiO_2 nano-particles. After the completion, the DSSC system was activated with a light source of (55-watt xenon lamp) that was set up in a 500 W/m^2 solar simulator. This lamp emits almost the same wavelengths as sunlight The testing temperature was 23^oC-25^oC. The performance of the cell was measured with a digital multi-meter (Agilent 34401).

2.3. The Theoretical Part

2.3.1. Band Gap Energy

The band gap energies of dye complexes were calculated using Equation (1) for a direct band gap of charge carried from allowed energy levels. Band gap energy of the TiO_2 samples can be acquired by using Tauc law [16]:

$$(\alpha hv) = \mathcal{A}(hv - Eg)^n \quad (\mathbf{1})$$

where: α represents the absorption coefficient, E_g represents absorption band gap energy, hv represents incident photon energy, $\mathcal{A}$ represents the corresponding constant of absorption, and n is a number that represents the mode of optical transmission.

2.3.2. Cell Efficiency

The ratio of the electrical power output to the power of incident radiation (P_{in}) is known as the cell's conversion efficiency. Eq. 2 was used to calculate the efficiency(η) of converting solar energy to electricity [17]:

$$\eta = \frac{FF \times J_{SC} \times V_{OC}}{P_{in}} \times 100\% \quad (\mathbf{2})$$

In this case, the lighted cell is short-circuited to acquire the short circuit current density (I_{sc}), whereas the open circuit voltage (V_{oc}) is produced when the circuit is open and no current can pass through it [18].

Another important indicator used to quantify the PV performance of a DSSC is the fill factor (FF), which is defined as the ratio of the maximum output power of the solar cell to its theoretical maximum power and whose value is always less than unity [19].

3. Results and Discussion

3.1. X-ray Diffraction (XRD)

The XRD patterns, obtained with an X-ray diffractometer, displayed in Fig. 1, were used to examine the crystalline structure of the manufactured samples (undoped and Mn-doped TiO_2 thin films of different Mn doping ratios) after two hours of heating at 500°C [20]. These patterns suggested the creation of the TiO_2 with anatase phase, as eight peaks were found attributed to this crystalline phase. Fig. 1 indicates that all samples have an anatase phase, and this is a good result for DSSCs application because anatase is more active in sunlight harvesting. The peaks correspond to the crystal planes (101), (200), (004), (211), (105), (116), (204), (220), and (215). The peak at 2θ=25.28°, belonging to the undoped TiO_2, was used as a reference to introduce the effect of Mn doping. TiO_2 samples were doped with various amounts of Mn (0, 1, 3, 5and 9%) [21]. The peak positions of the undoped and Mn-doped TiO_2 thin were identical supporting the formation anatase phase. Table (1) lists the data obtained from the XRD analyses on different Mn-doped samples of titanium and the crystallite sizes calculated according to Scherer equations [22]:

$$D = \frac{k\lambda}{\beta\cos(\theta)} \qquad (3)$$

where: D denotes the size of crystallite (nm) of a material, K denotes form factor =0.90, λ represents X-ray wavelength (nm), β is the full width of half maximum intensity of the diffracted peak values (FWHM), and θ represents Bragg angle.

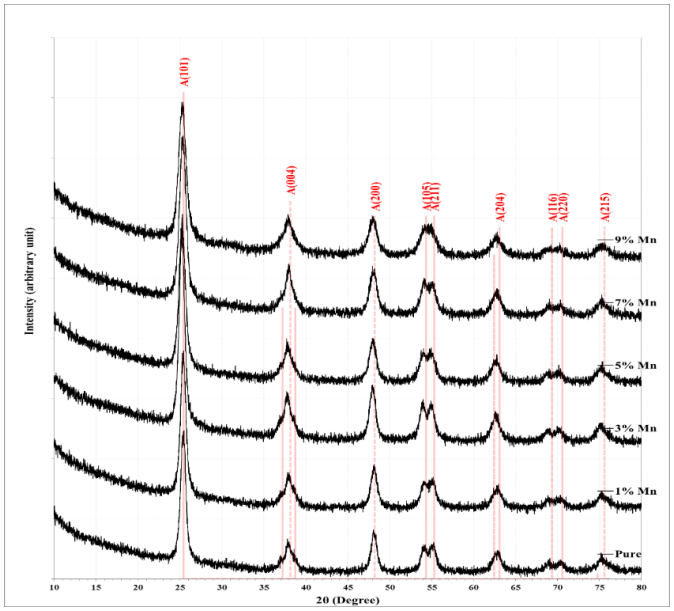

Figure 1: XRD patterns of undoped and Mn -doped TiO_2 Thin Film.

Table 1: Summary of the data obtained from the XRD analyses on different Mn-doped samples of titania.

Sample	Mn%	2θ (Deg.)	FWHM (Deg.)	d_{hkl} (Å)	D (nm)	Hkl	Phase
T	0	25.2886	0.3031	3.5190	26.9	(101)	AnataseTiO_2
TM1	1	25.2412	0.5628	3.5255	14.5	(101)	AnataseTiO_2
TM2	3	25.2432	0.6927	3.5252	11.8	(101)	AnataseTiO_2
TM3	5	25.2926	0.1732	3.5184	47.0	(101)	AnataseTiO_2
TM4	7	25.2744	0.4330	3.5209	18.8	(101)	AnataseTiO_2
TM5	9	25.4103	0.6494	3.5024	12.5	(101)	AnataseTiO_2

3.2. Measurements of AFM

Figs. 2-7 show the 2D and 3D AFM images of undoped and manganese-doped TiO_2 at manganese ratios of (1% - 9%) calcined under a steady degree temperature. They showed that the products consist of small particles. At 500^{o}C, it is clear that all doped and undoped samples have smooth granular surfaces and nano-structure particle size. Table 2 lists the average surface roughness (RMS) for these films, where the values varied between 49.38nm and 58.57nm and the maximum roughness rate was 7% with a minimal of 0%. The same result was reported by Sharma et al. [23].

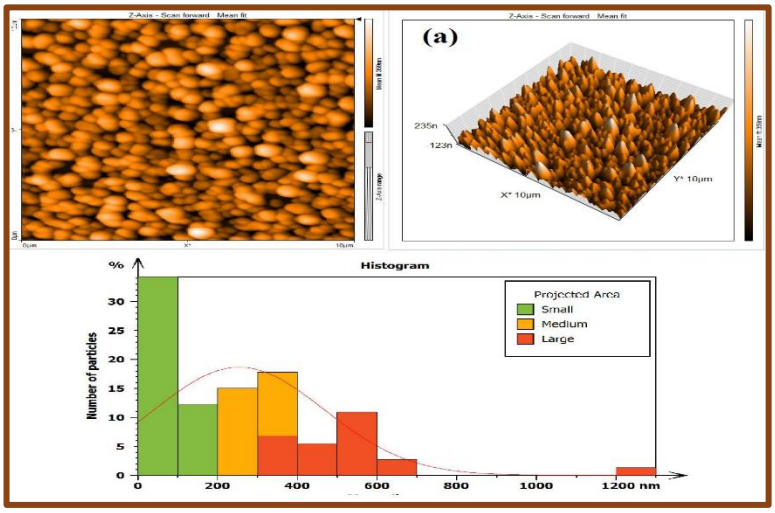

Figure 2: AFM images for TiO_2 (a) undoped (2D) (b) undoped (3D) (c) Histogram Nano- particles.

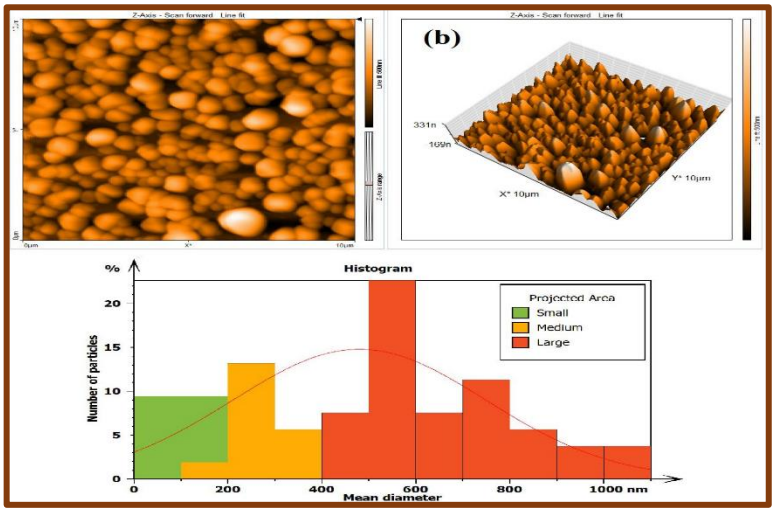

Figure 3: AFM images for TiO_2 (a) TM1 (2-D) and TM1 (3-D) and Histogram Nano-particles

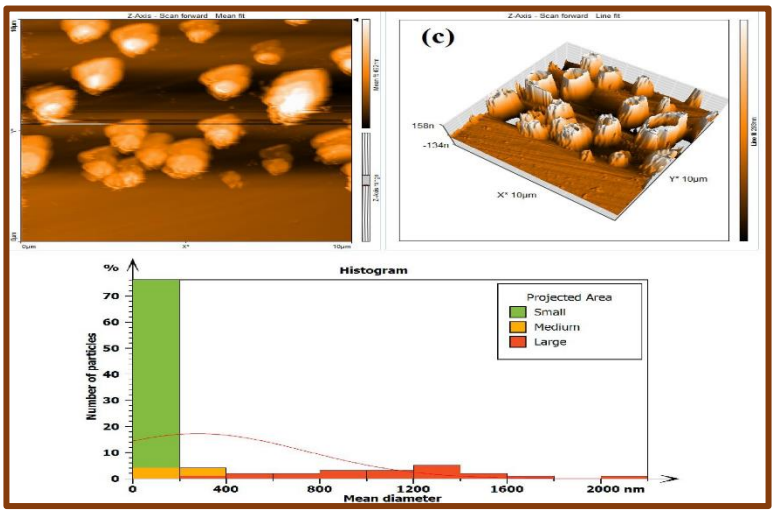

Figure 4: AFM (a) 2D and (b) 3D images for TM2 sample Mn-doped TiO_2 (c) Histogram nano-particles.

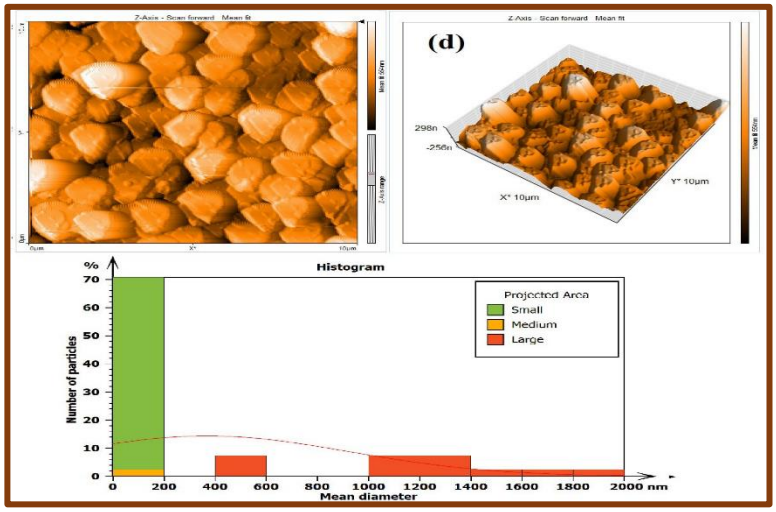

Figure 5: AFM (a) 2D and (b) 3D images for TM3 sample Mn-doped TiO_2 (c) Histogram nano-particles.

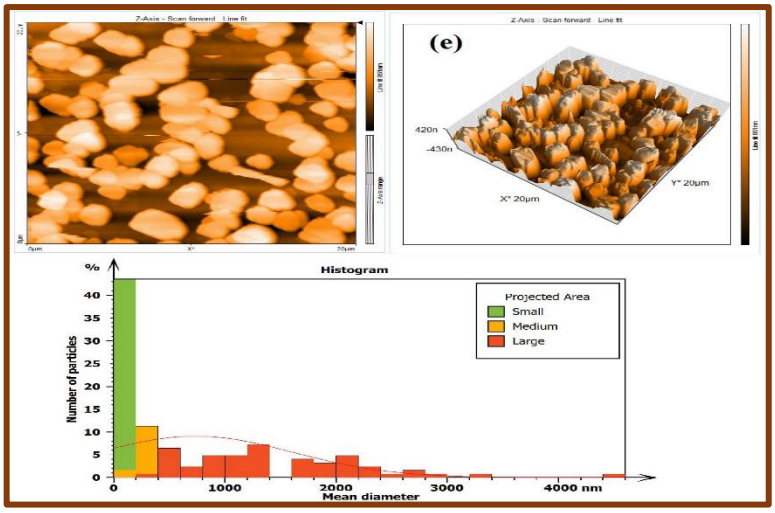

Figure 6: AFM (a) 2D and (b) 3D images for TM4 sample Mn-doped TiO_2 (c) Histogram nano-particles.

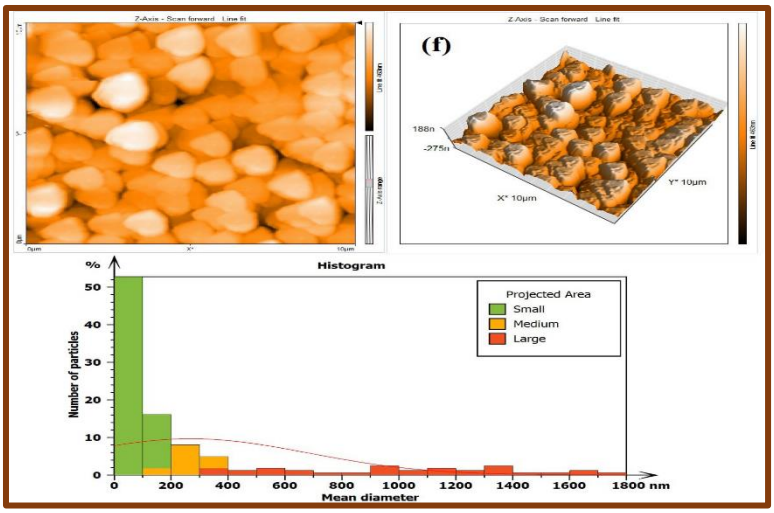

Figure 7: AFM (a) 2D and (b) 3D images for TM5sample Mn-doped TiO_2 (c) Histogram nano-particles.

Table 2: **Values obtained from AFM images of the undoped and Mn-doped TiO_2 thin films nano-particles.**

Sample	Mn wt%	Average diameter (nm)	RMS Roughness (nm)	Roughness Av(nm)	Height (nm)
T	0	254.0	62.65	49.38	453.9
TM1	1	479.5	79.26	63.14	489.8
TM2	3	277.9	97.96	70.32	1542
TM3	5	368.3	86.63	67.83	763.1
TM4	7	735.3	208.2	188.7	1680
TM5	9	268.0	73.2	58.57	520.5

3.3. UV–Visible Spectroscopy

Fig. 8 shows the UV-Visible spectral absorption spectra of the undoped and Mn-doped TiO_2 with various concentration levels of manganese. It can be noticed that the undoped TiO_2 had mainly absorbed the ultra-violet light of < 390 nm wavelength, which corresponds to the electronic excitation from the valence band to the conduction band across an energy gap value of 3.2 eV. With the increase of Mn dopant concentrations, the edge of absorption had shifted toward indirect optical length values (i.e., redshift). The energy band gap was reduced with the increase of the doping 9% doping was attained, and there was visible optical uptake spread. Using the infrared spectral spectrum and that has been discovered to be consistent with the data. This has shown that the replacement of red optical absorption changes of titanium ions by the ions of manganese in TiO_2 matrix characteristics and in general, leads to the band gap reduction [24].

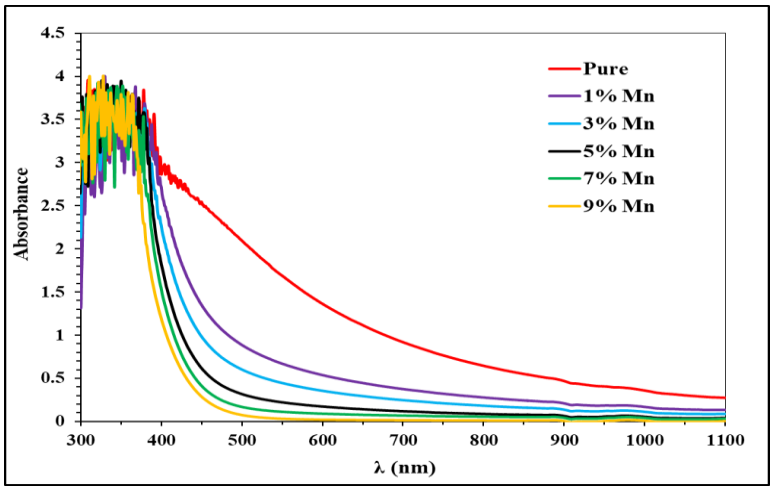

Fig. 8: UV-Vis absorbance spectra of the undoped and Mn-doped TiO_2 with different concentration of manganese.

3.4. The Band Gap Energy Calculations

The band gap energy of the undoped and Mn-doped TiO_2 with different concentration of manganese were derived from Tauc plots, as shown in Fig. 9. Table 3 lists the values of the band gap energies, from which it can be noted that the band gap energy decreased with the increase of the Mn-doping level. It decreased in the direction of the absorption edge movements (red shifting) until the 7% concentration and returns afterward (i.e., the blue shifting), and this is proper for the photocatalytic implementations.

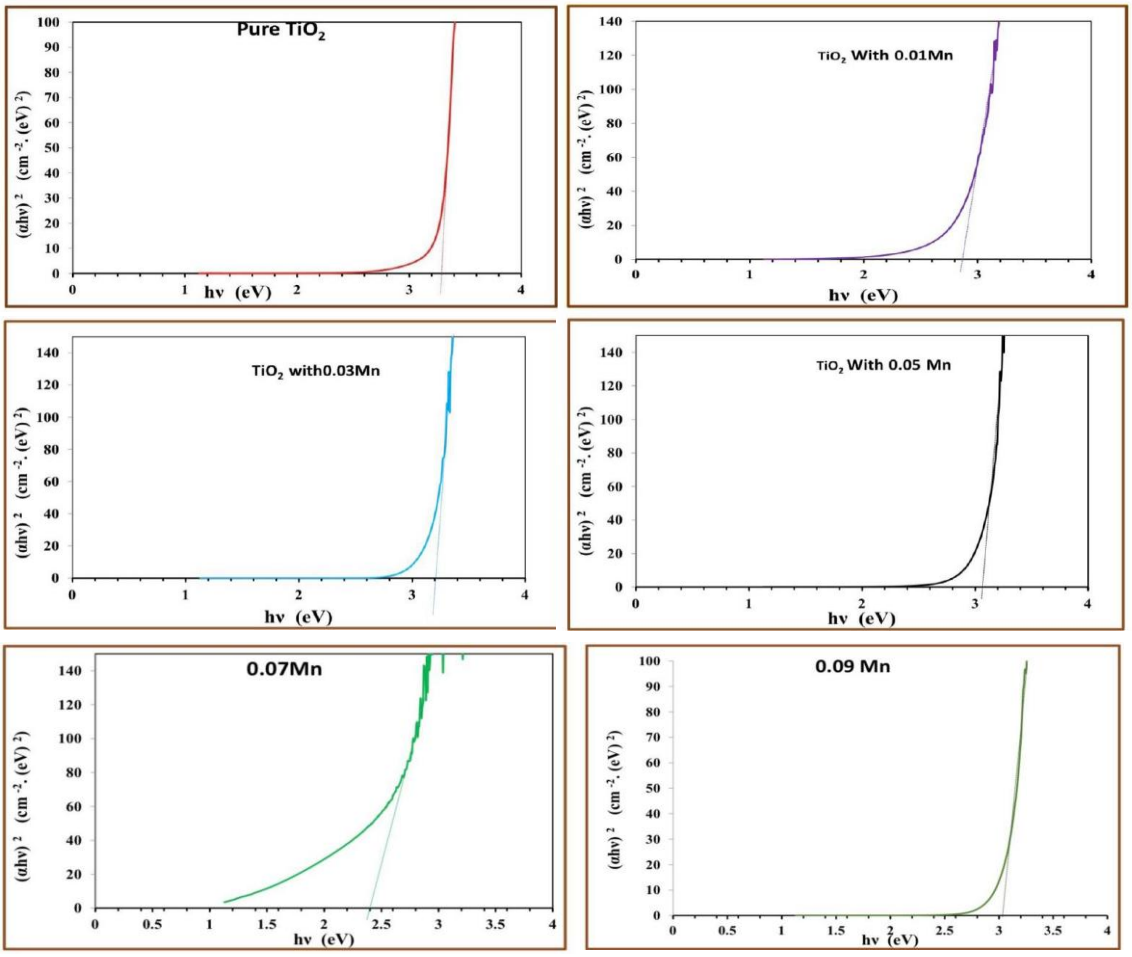

Figure 9: Tauc plots of the undoped and manganese-doped TiO_2.

Table3: Band-gap values of TiO_2 undoped and Mn-doped samples.

Sample	Mn wt%	Eg (eV)
T	0%	3.2
TM1	1%	2.8
TM2	3%	3.1
TM3	5%	3.0
TM4	7%	2.4
TM5	9%	3.1

3.5. Field-Emission Scanning Electron Microscopy (FE-SEM)

Fig. 10 shows the FE-SEM images (of 500 nm images scale). FE-SEM was utilized to analyze the surface profile and particle size of the synthesized thin films, which are suitable for photo catalysts in undoped Mn and doped with doping ratios of (1, 3, 5, 7 and 9%). They show uniformly homogeneous growth of the TiO_2 films. Detailed FE-SEM observations have revealed that the pattern of heat is composed of thin interconnected cracks of different lengths and orientations due to the oxide-scale cracking under thermal stresses. This is due to cyclic transition thermal gradients induced by repeated heating and cooling of the surface. When doping with Mn of different weight percentages (1, 3, 7, and 9%) noticeable or distinct circles emerge, signifying the existence of adsorption. These images make it evident that such samples contain distinct crystals of various shapes and sizes. There's no denying that crystals adapted specific geometric forms. The homogeneity regarding the particle distribution is the distinguishing characteristic that could be seen in these images. Additionally, one of the most significant benefits of the sol-gel technique employed in the production of thin films is the extremely small particle size [25]. It can also be observed in some samples that there is no aggregation on the sample, and the interlayer distance between the nanoparticles is very small, so the surface area has increased significantly. Therefore, the photo catalytic efficiency was enhanced. The nanoparticles size was recorded from the scale images at (500 nm) using image analysis software, as listed in Table 4. The size for undoped TiO_2 was 21.36nm. In Mn-doped TiO_2 samples, the nanoparticle sizes were 21.36, 32.77, and 21.36nm for the TM1, TM2, and TM3, respectively, while it was 14.27 for the TM4 sample (corresponding to 0.12mol Mn), indicating more uniformity than the undoped TiO_2, which is suitable for photocatalysis performance. The values of the mean particle sizes are listed in Table 4. It was also found that the measured surface roughness average values (Table 2) were large, which indicates the possibility of using these films in solar cells or using them to increase the absorption of film to photons of energy [26].

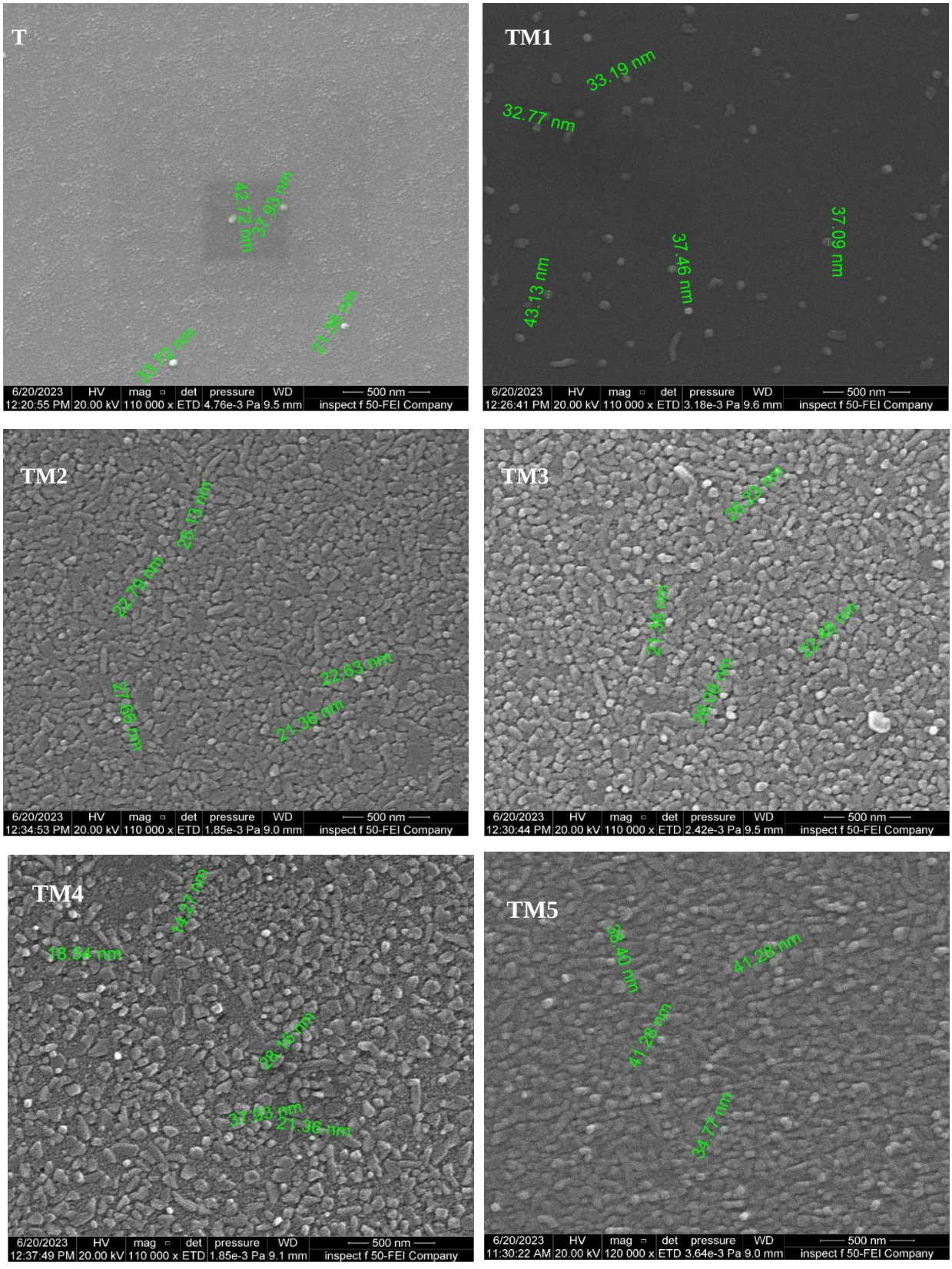

Figure13: FE-SEM images of TiO_2 at (500nm) scale.

Table 4: The mean particle size of the undoped and Mn-doped TiO_2 of different doping percentages obtained from the FE- SEM analysis.

Samples	Mn wt%	Mean Particle size (nm)
T	0	21.36
TM-1	1	21.36
TM-2	3	32.77
TM-3	5	21.36
TM-4	7	14. 27
TM-5	9	34.77

3.6. Effect of Doping on DSSC Efficiency

The J–V curve characteristics represent the relation between current and voltage. Fig. 11 shows the J-V characteristics of the DSSC of the pure and 7 % Mn-doped TiO_2 doped TiO_2 working electrode in the case of utilizing Rhodamine B dye. The efficiency of DSSC was calculated for these cells, as shown in Table 5.

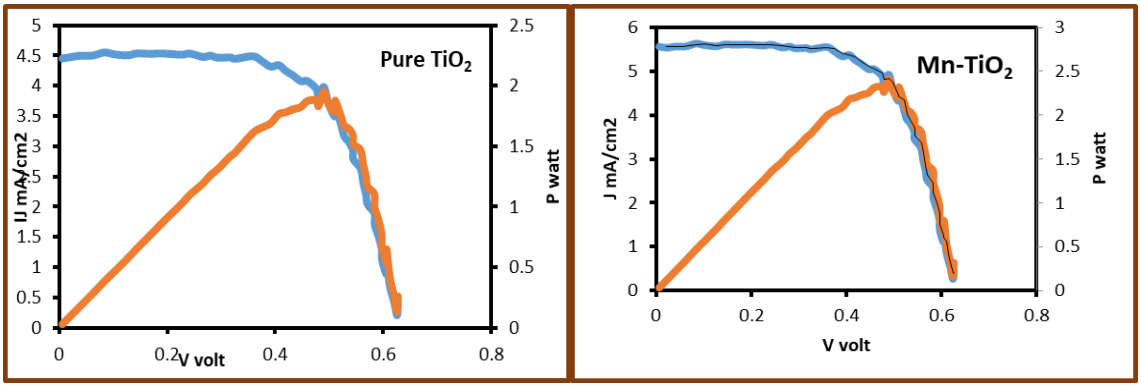

Figure 11: The J-V curve Effect of doping on DSSC efficiency.

Table 5: the efficiency of undoped TiO_2 and optimum Mn-doped TiO_2.

Sample	V_{max} (V)	I_{max} (mA)	F.F%	η%
Undoped	0.489	3.94	68.50347	0.488092
Mn-TiO_2	0.488	4.965	68.45954	0.604074

5. Conclusions

This work successfully prepared undoped, Mn-doped TiO_2-NPs using the sol-gel approach. It was found that employing (Mn) doped titanium as the working electrode in the DSSC enhanced the solar cells' power conversion efficiency. The band gap energy decreased as the Mn percentage doping of TiO_2 increased, causing the absorption edge to shift to a higher energy level.

Acknowledgments

The authors acknowledge their thanks to the Environmental Laboratory in the College of Science, Department of Chemistry, for completing this research work.

Conflict of interest

Authors declare that they have no conflict of interest

References

1. K. Sharma, V. Sharma, and S. S. Sharma, Nanosc. Res. Lett. **13**, 381 (2018).
2. F. H. Ali, Iraqi J. Phys. **16**, 28 (2018).

3. A. Bartkowiak, O. Korolevych, G. L. Chiarello, M. Makowska-Janusik, and M. Zalas, Appl. Surf. Sci. **597**, 153607 (2022).
4. T. Stergiopoulos, E. Rozi, C.-S. Karagianni, and P. Falaras, Nanosc. Res. Lett. **6**, 307 (2011).
5. C.-P. Lee, C.-T. Li, and K.-C. Ho, Mater. Today **20**, 267 (2017).
6. F. J. Al-Maliki and M. A. Al-Rubaiy, Opt. Quan. Elect. **54**, 377 (2022).
7. M. A. Nima and F. J. Kadhim, Iraqi J. Appl. Phys. **17**, 9 (2021).
8. M. M. Mohsin and F. H. Ali, Chem. Methodol. **7**, 335 (2023).
9. A. H. Hasan and F. Hasan, Indian J. Nat. Sci. **9**, 15242 (2018).
10. A. M. Alqudsi and K. A. Saleh, Baghdad Sci. J. **21**, 1243 (2024).
11. K. Mangersnes, PhD Thesis, University of Oslo, 2011.
12. N. E. Martínez and P. Cart, PhD Thesis, University of Bretagne Loire, 2012.
13. A. S. Al-Ezzi and M. N. M. Ansari, 5 **5**, 67 (2022).
14. W. A. Al-Taa'y and B. A. Hasan, Iraqi J. Phys. **19**, 22 (2021).
15. R. Su, R. Bechstein, J. Kibsgaard, R. T. Vang, and F. Besenbacher, J. Mater. Chem. **22**, 23755 (2012).
16. R. Wang, K. Hashimoto, A. Fujishima, M. Chikuni, E. Kojima, A. Kitamura, M. Shimohigoshi, and T. Watanabe, Nature **388**, 431 (1997).
17. B. Pradhan, S. K. Batabyal, and A. J. Pal, Sol. En. Mater. Sol. Cell. **91**, 769 (2007).
18. F. Arjmand and Z. R. Ranjbar, Heliyon **8**, e11692 (2022).
19. J. Halme, MSc Thesis, Helsinki University of Technology, 2002.
20. A. A. Salman, MSc Thesis, Al-Nahrain University, 2012.
21. A. A. Al-Khafaji, D. B. Alwan, F. H. Ali, and W. Twej, Envir. Sci. Indian J. **12**, 217 (2016).
22. S. N. R. Inturi, T. Boningari, M. Suidan, and P. G. Smirniotis, Appl. Cat. B Envir. **144**, 333 (2014).
23. S. Sharma, S. Chaudhary, S. C. Kashyap, and S. K. Sharma, J. Appl. Phys. **109**, 083905 (2011).
24. M. M. Abbas and M. Rasheed, Iraqi J. Phys. **19**, 1 (2021).
25. F. H. Ali, Journal of Physics: Conference Series (IOP Publishing, 2021). p. 012076.
26. N. M. Jabbar and M. M.-A. Hussein, Iraqi J. Phys. **20**, 109 (2022).

دراسة الخصائص البصرية والهيكلية لقطب ثنائي أوكسيد التيتانيوم المطعم بالمعادن بطريقة السول – جل في الطاقة الشمسية الحساسة للصبغة

هديل دخيل حمدالله[1] وفلاح حسن علي[1]

[1] قسم الفيزياء، كلية العلوم، جامعة بغداد، بغداد، العراق

الخلاصة

في هذه الدراسة تقديم استراتيجية لزيادة كفاءة الخلايا الشمسية الحساسة للصبغ عن طريق تطعيم ثنائي أوكسيد التيتانيوم بالمنغنيز بطريقة (السول-جل) واستخدمت بنجاح كأنود ضوئي للخلايا الشمسية الحساسة للصبغة. تم دراسة خصائص ثنائي أكسيد التيتانيوم غير مطعم والمطعم بالمنغنيز باستخدام تقنية حيود الاشعة السينية. واظهرت القياسات وجود طور الانتس في كل الافلام الرقيقة. يتغير امتصاص طيف الاشعة الفوق البنفسجية والمرئية مع ازدياد تراكيز ثنائي اوكسيد التيتانيوم مع المنغنيز (1% , 3% , 5% ,7% ,9%) يشير الى حدوث انتقال نحو المنطقة المرئية. لـــــذلك تتناقص فجوة الطاقة مع زيادة التطعيم. الحد الأدنى لقيمة فجوة الطاقة (2.4 فولت) بوزن 7٪. أظهرت قياسات المجهر الإلكتروني الماسح أن حجم جسيمات الأفلام الرقيقة يقل مع عملية التطعيم ويصل إلى قيمة دنيا عند نـــــسبة التطعيم بنسبة 7%. تم فحص العينات باستخدام حيود الأشعة السينية لتحديد حجم الحبيبات قبل وبعد التطعيم مع المنغنيز. أكسيد التيتانيوم المطعم بالإنديوم مغطى بطبقة رقيقة زجاجية باستخدام طريقة doctor Bladeالسماكة المثالية لعجينة (انديوم اوكسيد تتانيوم) فوق الزجاج الموصل هو (15 ميكرومتر)، كفاءة التحويل للقدرة تتزايد الى 0.604074 % وتيار الأعظم 4.965 مل امبير وفولطية العظمى 0.488 فولت وعامل التصحيح للكفاءة هو 68.45954%.

الكلمات المفتاحية: تطعيم منغنيز، صبغة روداميـن ب، ثنائي أوكسيد التيتانيوم، الخلايا الشمسية الصبغية الحساسة، الكفاءة.